Impact of Amine Additives on Perovskite Precursor Aging: A Case Study of Light-Emitting Diodes

Yan Xu,[a,b] Weidong Xu,[b]* Zhangjun Hu,[b] Julian A. Steele,[c] Yang Wang,[d] Rui Zhang,[b] Guanhaojie Zheng,[b] Heyong Wang,[b] Xin Zhang,[b] Eduardo Solano,[e] Maarten B. J. Roeffaers,[c] Kajsa Uvdal,[b] Jian Qing,[b, f] Wenjing Zhang,[a]* and Feng Gao[b]*

[a] International Collaborative Laboratory of 2D Materials for Optoelectronics Science and Technology of Ministry of Education Institute of Microscale Optoelectronics, Shenzhen University, Shenzhen 518060, China.

[b] Department of Physics Chemistry and Biology (IFM), Linköping University, Linköping SE-58183, Sweden.

[c] cMACS, Department of Microbial and Molecular Systems, KU Leuven, 3001 Leuven, Belgium.

[d] Key Laboratory for Organic Electronics and Information Displays, Institute of Advanced Materials (IAM), Jiangsu National Synergetic Innovation Center for Advanced Materials (SICAM), Nanjing University of Posts & Telecommunications, 9 Wenyuan Road, Nanjing 210023, China.

[e] NCD-SWEET beamline, ALBA synchrotron light source, 08290, Cerdanyola del Vallès, Barcelona, Spain

[f] Guangzhou Key Laboratory of Vacuum Coating Technologies and New Energy Materials, Siyuan Laboratory, Department of Physics, Jinan University, Guangzhou 510632, P. R. China.

* Email: weidong.xu@liu.se; wjzhang@szu.edu.cn; feng.gao@liu.se

ABSTRACT: Amines are widely employed as additives for improving the performance of metal halide perovskite optoelectronic devices. However, amines are well-known for their high chemical reactivity – the impact of which is yet to receive detailed handling in the community of perovskite light-emitting diodes. Here, by investigating an unusual positive ageing effect of $CH_3NH_3I/CsI/PbI_2$ precursor solutions as an example, we reveal that amines gradually undergo *N*-formylation reaction in perovskite precursors over time. This reaction is initialized by hydrolysis of dimethylformamide (DMF) in the acidic chemical environment. Further investigations suggest that the reaction products collectively impact perovskite crystallization and eventually lead to significantly enhanced EQE values, rising from ~2% for fresh solutions to over ~12% for aged ones. Our findings pave the way for more reliable and reproducible device fabrication, and call for further attention to underlying chemical reactions within the perovskite inks once amine additives are included.

TOC figure

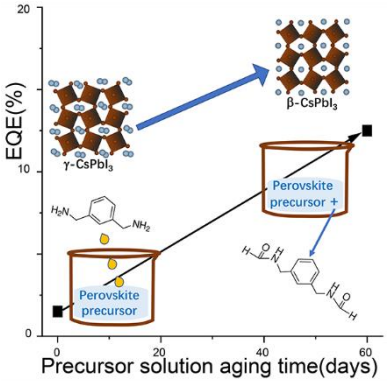

Intense research into metal halide perovskites has led to great advances in solution-processed optoelectronic applications such as photovoltaics, photodetectors and light-emitting diodes.[1-5] In addition to the development of various advanced thin-film processing techniques, the remarkable progress in the performance of perovskite optoelectronic devices greatly benefits from compositional engineering.[6-8] State-of-the-art perovskite inks usually have complex compositions which include not only the necessary combinations of organic/inorganic salts for constructing perovskite structures, but also a wide range of additives for improving device performance.[9-11] Among the additive, amines are the most intensively investigated in perovskite optoelectronic devices.[12-15] Various functionalities and advantages, such as defect passivation, crystallization control and morphological optimization, have been clearly identified.[16-20] In particular, additive engineering with amines has recently boosted the external quantum efficiency (EQE) values of perovskite light-emitting diodes (PeLEDs) to over 20%.[21-23]

In spite of these positive effects, it is well known that amines are highly reactive, and also sensitive to heating and light exposure. The high chemical reactivity and poor stability of amines can potentially introduce a variety of chemical reactions into the precursor solutions, leading to permanent changes in solution constituents. This is in line with the common observations that the quality of perovskite films is strongly dependent on the shelf storage time of precursor solutions.[24] Given that additive engineering with amines has become an area of focus in perovskite optoelectronic devices, a detailed understanding of the chemistry within the precursor inks is of critical importance for reliable and reproducible device fabrication.

Here, we reveal the underappreciated chemical reactivity of amine additives in the precursor solution which significantly affects perovskite crystallization and hence the performance of PeLEDs. We find that *N*-formylation of amino groups occurs and is accompanied by dimethylformamide (DMF) hydrolysis during solution storage. These reactions are driven and accelerated not only by heating, but also through the acidic environment in the solution due to the presence of methylammonium (MA^+) and/or formamidinium (FA^+) halides. It gives rise to continuous changes in the constituents of the solution with increasing shelf storage time and thus varied device performance. Notably, although this behaviour may be destructive in most scenarios, we show that the resultant products in $CH_3NH_3I/CsI/PbI_2$ precursor inks are able to boost the performance of PeLEDs, resulting in a remarkable EQE enhancement from ~2% to ~12%.

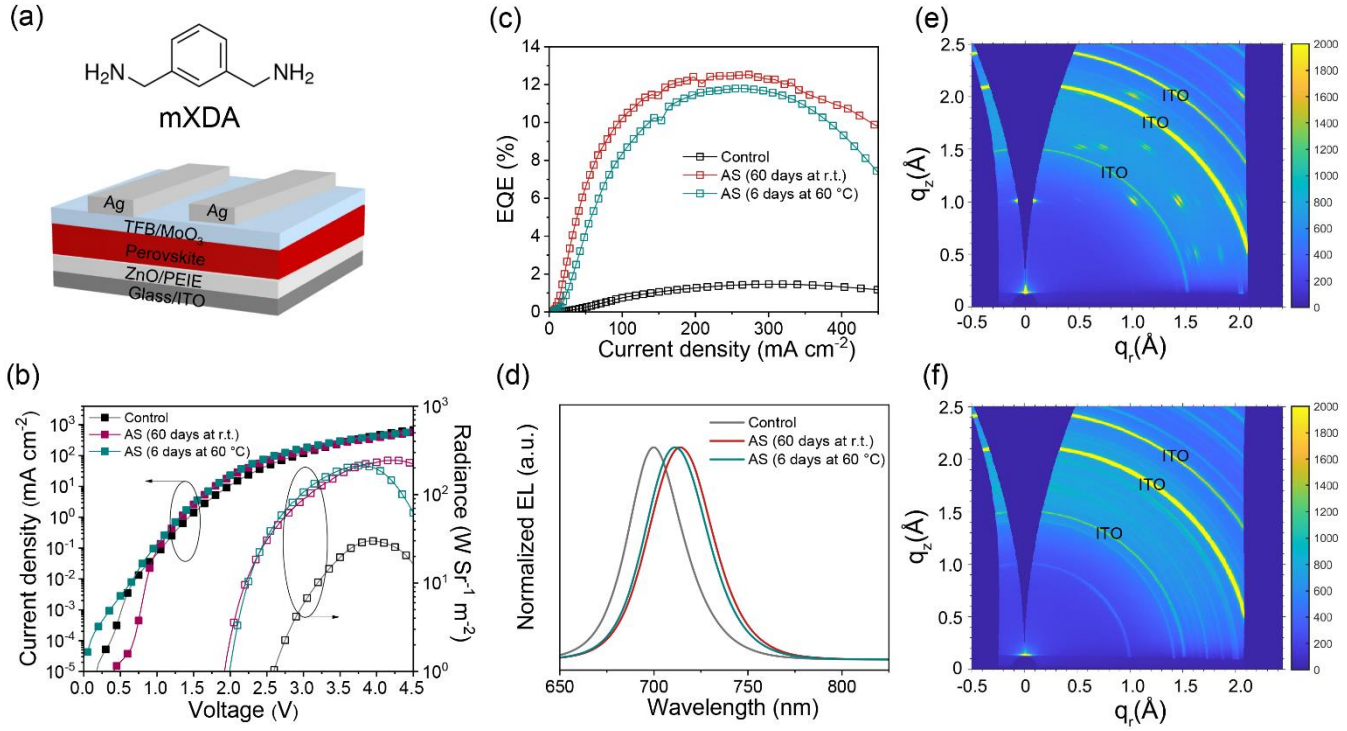

Figure 1. a) Molecular structure of mXDA and device architecture. b-d) Device characteristics for mXDA control devices and aged-solution (AS) counterparts (stirring for 60 days at r.t. and 6 days at 60 °C): Current density-voltage-radiance (J-V-R) (b); Current density-EQE (J-EQE) (c); EL spectra (d). e-f) 2D GIWAXS patterns for control (e) and AS perovskite films (f).

We fabricate PeLEDs by subsequent deposition of zinc oxide nanocrystals (ZnO NCs)/polyethyleneimine ethoxylated (PEIE) /perovskites/poly(9,9-dioctylfluorene-co-N-(4-(3-methylpropyl)) diphenylamine (TFB)/MoO_3/Ag on patterned indium tin oxide (ITO) substrates (Fig. 1a). The perovskite emissive layers are deposited by spin-casting the precursor inks with a stoichiometry of PbI_2: CsI: MAI = 1: 1.15: 1. We select m-xylylenediamine (mXDA) (Fig. 1a) as the additive with a stoichiometry of 0.6 equivalent of lead cations. The PeLED devices prepared from fresh and aged precursor solutions are referred to as control and aged-solution (AS) devices, respectively. Unless otherwise stated, the aged solutions have been stirred at 60°C for at least 6 days before use.

Fig. 1b-1d display the representative characteristics of devices prepared from aged precursors stored at room temperature for 60 days and that at 60°C for 6 days, respectively. The control devices prepared from fresh solutions are investigated for comparison. Intriguingly, both ageing processes give rise to considerable improvements in the figure of merits of the device in terms of peak EQE values, maximum radiance as well as reduced turn-on voltages. Specifically, both AS devices show peak EQE around 11~12%, which contrasts sharply to the control cases showing a low value of ~2% (Fig. 1c). The control devices show EL spectra peaking at 700 nm which is comparable to the emission from all-inorganic γ-

$CsPbI_3$. It indicates that MAI is hardly retained in the perovskite films due to their volatile property at the high temperature (150 °C for annealing) and the deprotonation ability of ZnO layer.[25]

Accompanied by the changes in device performance with shelf storage time, the EL peaks shift toward longer wavelength (from 700 to 716 nm) (Fig.1d). The Tauc plots of the perovskite films (Fig. S1) confirm that the EL shifts arise from a reduced bandgap from 1.74 eV for control films to 1.71 eV for AS cases.

We show the 2D grazing incidence wide angle X-ray scattering (GIWAXS) patterns of control and AS perovskite films in Fig. 1e and 1f respectively. Distinct from control films which give discrete Bragg spots, the AS films show randomly distributed crystalline orientations for all respective Debye-Scherrer rings.

Together, the above-mentioned results are clearly indicative of continuous compositional variation in the perovskite precursor inks, leading to large differences in the perovskite crystallization process and relevant polycrystalline orientations. These discrepancies ultimately lead to significant variations in the optoelectronic properties of the perovskites and the device performance.

To rationalize the chemical processes underlying the positive ageing effect of the solutions, the first question that arises is which component(s) in the precursors undergo chemical reactions during storage. We investigate the organic components closely given that they are chemically less stable and more reactive than the inorganic compounds. First, we independently age MAI and mXDA in DMF and then mix each with the other fresh constitutes respectively to make the solutions for device fabrication. The characteristics of representative devices prepared from aged mXDA/fresh MAI, fresh mXDA/aged MAI are summarized in Fig. S2. However, no distinct improvement is found here compared to control devices.

We then mix MAI and mXDA in DMF for ageing and compare the device performance to the case of independently aged MAI and mXDA, aiming to figure out if the chemical processes within the inks involve both components. We show the device characteristics in Fig. 2a-2c. Ageing MAI/mXDA together not only leads to remarkable enhancements in EQE values of reaching ~12%, but also red-shifted EL spectra (712 nm in this case). In contrast, independently aged MAI and mXDA display moderate performance improvements. In addition, compared to the use of fresh solutions (Fig. 1d), no EL shift is visible.

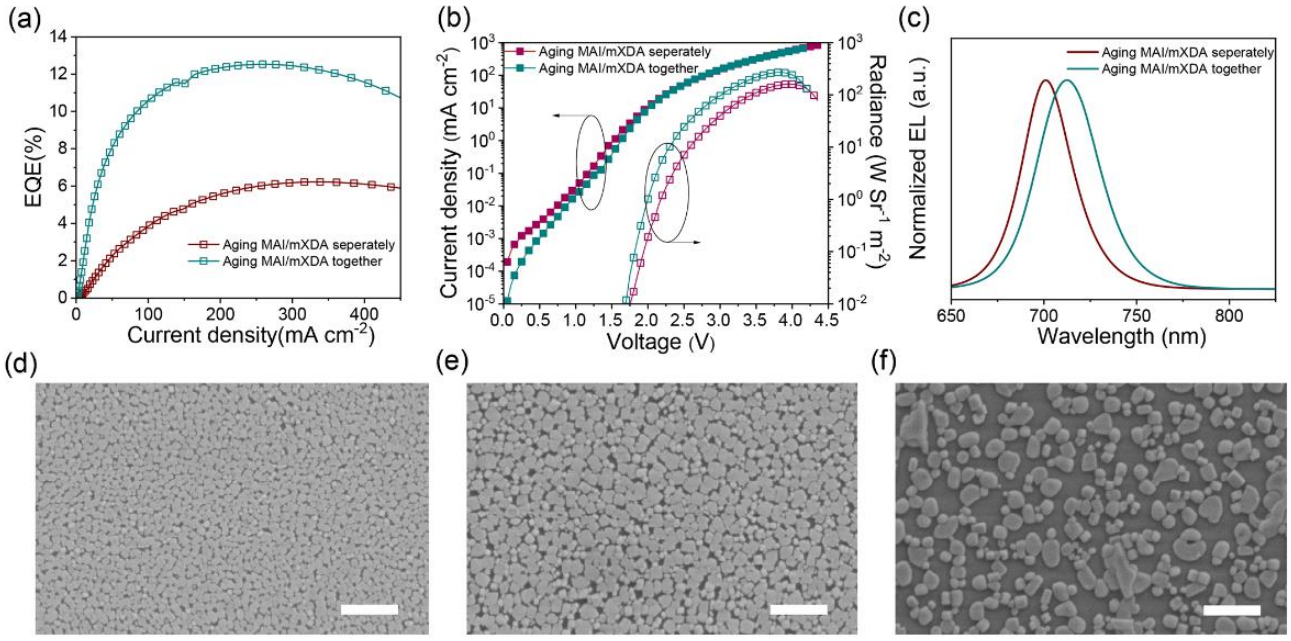

Figure 2. a-c) Characteristics for devices prepared from aged MAI/mXDA mixture and independently aged MA and mXDA in DMF: J-EQE (a); J-V-R (b); EL spectra (c). d-f) SEM images for perovskite films prepared from fresh solution (d), separately aged MAI and mXDA solutions (e), aged MAI/mXDA mixed solutions (f). The scale bar is 1 μm.

Consistently, the morphological evolutions of the perovskite layers indicate that the underlying chemical processes involve mXDA and MAI simultaneously. The mXDA control films show nanoscale grain sizes and relatively dense surface coverage (Fig. 2d). A similar morphology is also visible in the film prepared from independently aged MAI and mXDA, though with slightly larger perovskite grains (Fig. 2e). In comparison, ageing MAI/mXDA mixtures leads to much-enlarged grain sizes and a discontinuous nano-island feature (Fig. 2f), indicating a significant change in the crystallization process. Previous reports have suggested that the discontinues surface coverage may benefit for improving PeLED performance due to enhanced light-out coupling efficiency, once the issue of leakage current can be well addressed.[22, 23] On the basis of all the above results, we conclude that the chemical process during solution ageing is a synergistic effect of MAI and mXDA in DMF, which changes the crystallization process and thus results in distinct improvements in device performance.

We thus investigate the chemical reactions within the MAI/mXDA DMF solutions more closely and perform high-performance liquid chromatography-mass spectrometry (HPLC-MS) to monitor the compositional evolution with storage time. Intriguingly, no signals of mXDA can be detected in the aged samples. Instead, the main components in aged samples show the main fragment with molecular weight of 193.2, which is 57 larger than that of mXDA (Mw = 136.2) (Fig. S3). In addition, to identify whether the reaction(s) involves DMF, we use deuterated DMF as the solvent for preparing the aged MAI/mXDA

sample. In this case, the molecular weight of the main product increases to 195.2 (Fig. S4), indicating that DMF also participates in the reactions.

In this regard, we infer that the main component detected in aged samples from HPLC-MS is most likely to be protonated *N*-(3-formylaminomethyl-benzyl)-formamide (FABF) ($[M+H]^+$ = 193.2) as a result of DMF hydrolysis and following *N*-formylation of mXDA. To verify this, we collect the main products of aged MAI/mXDA samples by preparative liquid chromatography (LC) and then perform nuclear magnetic resonance (NMR) tests. In addition, we synthesize FABF as the reference sample through a well-established *N*-formylation method.[26] The synthetic details are summarized in Supporting Information and Scheme S1. By comparing the ^{1}H and ^{13}C NMR data as shown in Fig. 3a and Fig. S5 respectively, we confirm that mXDA undergoes *N*-formylation reactions with formic acid, which eventually results in the formation of FABF. As above mentioned, MAI is also critical for the reactions within the precursors. Thus, we infer that MA^+ provides the acidic environment for accelerating DMF hydrolysis, and dimethylamine (DMA) forms as another product.[27] In addition, the consumption of formic acid and the production of water caused by the *N*-formylation reaction further promote DMF hydrolysis, facilitating the entire processes.

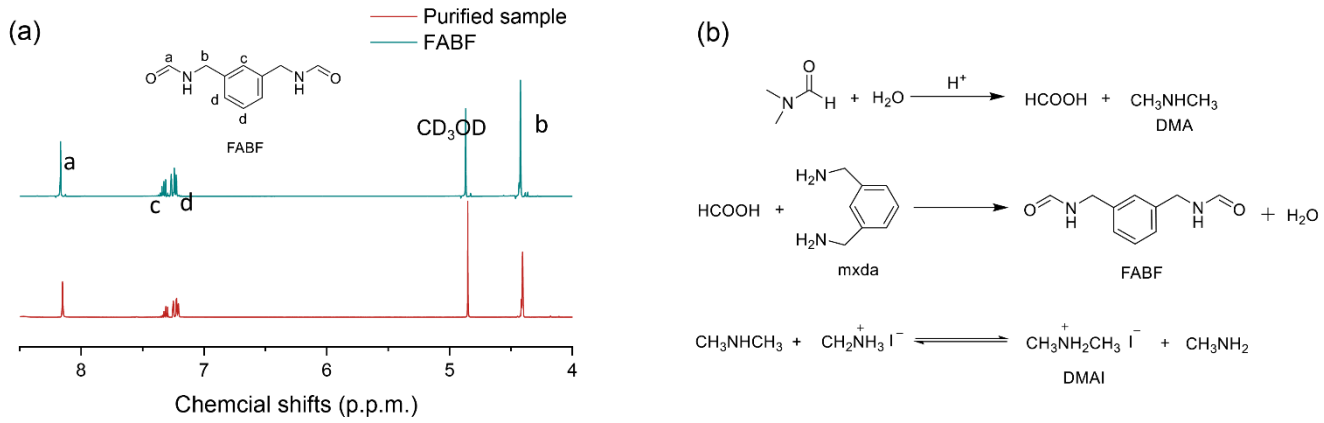

Figure 3. a) A comparison of ^{1}H NMR spectroscopy of purified products from aged MAI/mXDA DMF solution and FABF (inset). b) Proposed chemical reactions during precursor ageing.

Having revealed the DMF hydrolysis and *N*-formylation reaction during solution ageing, we use the reaction products (FABF and dimethylammonium iodide (DMAI)) as the additives to simulate the eventual components of aged inks and prepare PeLEDs, aiming to further validate our conclusions. We use DMAI since the protonation of *in-situ* formed DMA readily happens in the presence of excess MAI (Fig. 3b). In addition, DMA is in gaseous state at room temperature and hence hard to be blended into perovskite inks. The precursor stoichiometry of PbI_2: CsI: MAI: DMAI is 1: 1.15: 1 - *x*: *x*. The mole ratio of FABF is 0.6 equivalent to lead cations which is identical to that of mXDA used in above mentioned

devices. In Fig. 4a-4b we show the characteristics of devices with MAI (x = 0), DMAI/MAI (x = 0.4) as the organic components. We note that using FABF alone is enough to remarkably improve the peak EQE value up to 9.6%. By replacing a part of MAI with DMAI (x = 0.4), the peak EQE value can be further enhanced to 12.1%, which is as high as the mXDA AS devices shown in Fig. 1. The optimized devices show negligible current-efficiency roll-off, with no obvious EQE decrease until a large current density of ~700 mA cm^{-2}. This gives rise to a large radiance of 434 W sr^{-1} m^{-2}.

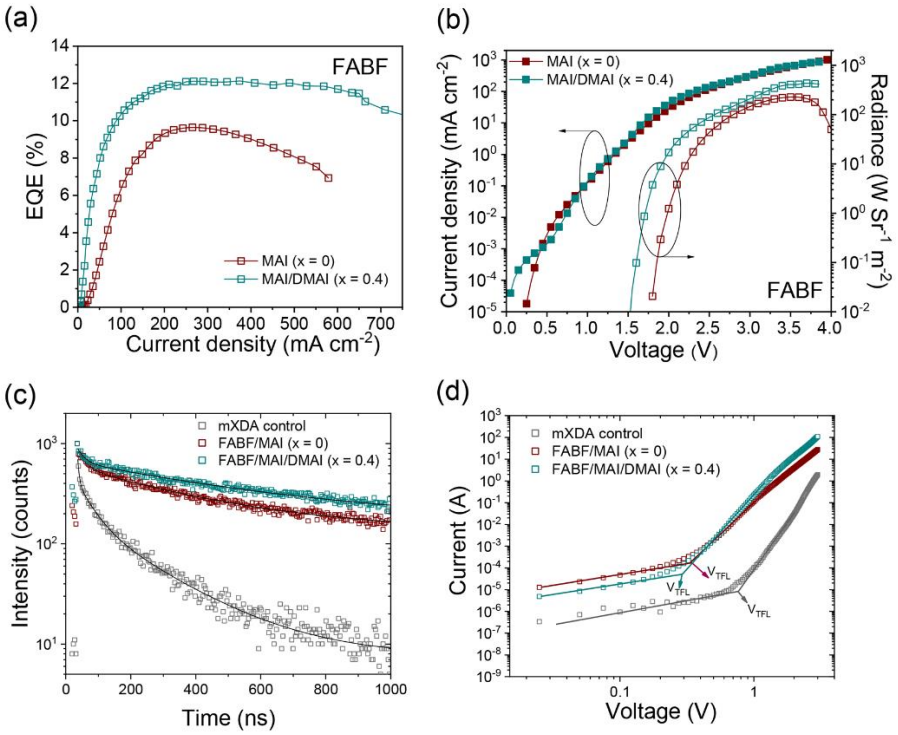

Figure 4. a-b) Characteristics for FABF- devices with MAI and MAI/DMAI (x = 0.4) as the organic cations: J-EQE (a); J-V-R (b). c) PL decay traces of mXDA control films, and that prepared by FABF/MAI and FABF/MAI/DMAI (x = 0.4) mixtures. d) The determination of V_{TFL} for probing trap density in the devices.

The performance enhancement can be attributed to reduced non-radiative recombination pathways, which is first evident by the remarkably prolonged PL lifetime as confirmed by time-correlated single photon counting (TCSPC) measurements (Fig. 4c). To further evaluate the discrepancies in the densities of traps (N_{dt}) within the devices, we measure the J-V curves of electron-only devices in the dark, with an architecture of ITO/ZnO/PEIE/perovskites/[6,6]-phenyl-C_{61}-butyric acid methyl ester ($PC_{60}BM$)/LiF/Al. The representative characteristics are shown in Fig. 4d, from which we observe a linear relation at low bias voltage followed by a nonlinear rise. The former corresponds to Ohmic response and the latter is assigned to the trap-filled limit regime with $J \propto V^n$ (n > 3). From the kink point (V_{TFL}), we deduce the value of N_{dt} according to the following equation:

$$V_{TFL} = \frac{eN_{dt}L^2}{2\varepsilon\varepsilon_0}$$

where L is the film thickness, e is the elementary charge, ε is the dielectric constant and ε_0 represent vacuum permittivity. The average trap densities determined from three devices are 1.5×10^{16} cm^{-3}, 6.4×10^{15} cm^{-3} and 5.9×10^{15} cm^{-3} for mXDA control films, FABF/MAI and FABF/MAI/DMAI films respectively. In addition to further reducing charge trapping, we note that the DMAI addition can effectively improve the charge injection, as suggested by the J-V curves of the single carrier devices. It could be one of the reasons for the high radiance and mitigated current-efficiency roll-off in the optimized FABF/MAI/DMAI devices (x = 0.4). As such, we conclude that the performance enhancements in mXDA-devices with prolonged solution ageing time are collectively contributed by the formation of FABF and DMAI, leading to mitigated trap-assisted non-radiative recombination and more efficient charge injection.

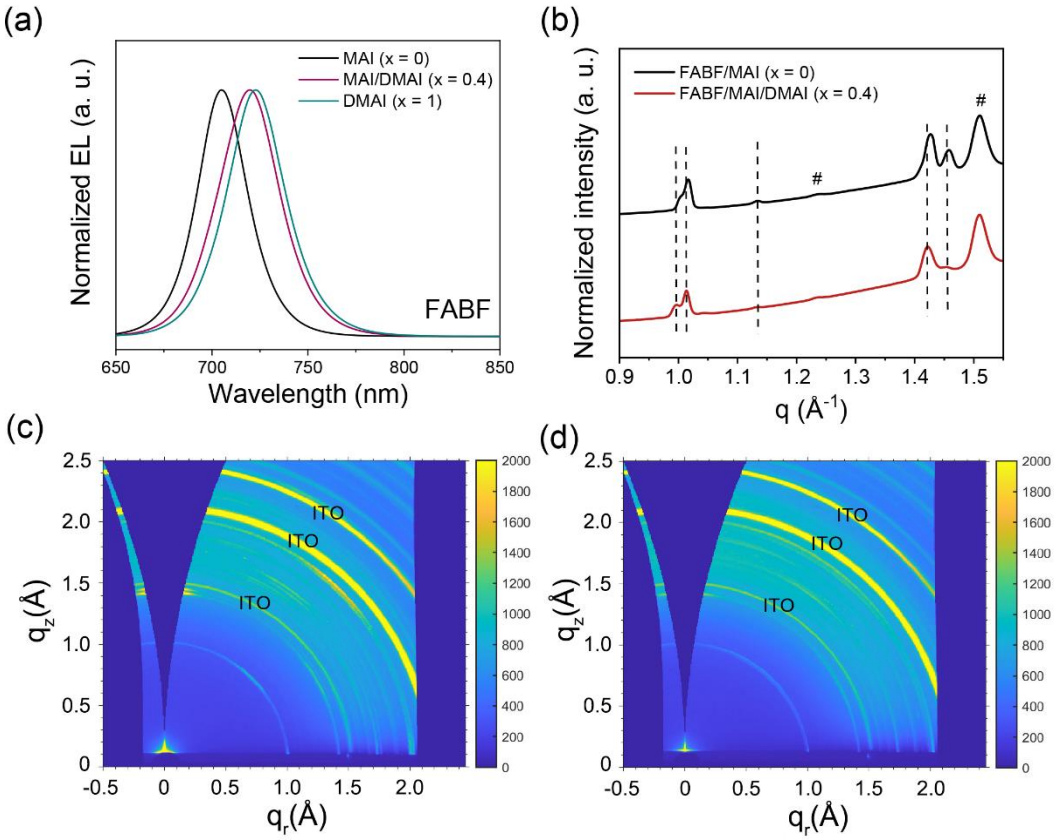

Figure 5. a) EL spectra for FABF-devices with MAI (x = 0), MAI/DMAI (x = 0.4) and DMAI (x = 1) in the precursor solution. b-d) 2D GIWAXS measurements for probing the crystal structure: Integrated scattering intensity profiles (b); 2D GIWAXS patterns for perovskite films prepared from FABF/MAI (c) and FABF/MAI/DMAI (x = 0.4) precursor solution (d). Here, # in Fig. 5b denote the diffraction peaks from ITO.

Notably, the EL spectra shift toward the longer wavelength with increasing DMAI content (from x = 0 to 1, Fig. 5a), analogous to the bandgap evolution observed in mXDA devices with prolonged solution ageing time. To identify whether FABF plays a key role in determining the bandgap as well, we prepare perovskite films without using FABF, that is, with a combination of DMAI: CsI: PbI_2: mXDA = 1: 1.15: 1: 0.6. As shown in Fig. S6, the optical bandgap determined by Tauc plot is 1.74 eV and the PL peak remains at 700 nm. In this scenario, the bandgap evolution of the perovskites during solution ageing is collectively caused by the production of both DMAI and FABF.

One possible explanation is that FABF and DMA cations together induce a shift in the crystal lattice symmetry and thus lead to a variation in bandgap. Similar observations can be found in recent work on perovskite photovoltaics where DMAI is used for stabilizing β-$CsPbI_3$ at room temperature with a reduced the bandgap.[28-30] We thus complete GIWAXS to characterize the crystal structure of FABF/MAI films with optimized DMAI addition (x = 0.4). We show the integrated X-ray scattering intensity profiles with q value ranging from 0.9~1.55 Å in Fig. 5b and 2D GIWAXS patterns in Fig. 5c-5d, respectively. The whole scattering patterns and their corresponding structural refinements are shown in Fig. S7a, from which we note that all the diffraction peaks of FABF/MAI films can be well assigned to orthorhombic γ-$CsPbI_3$. In comparison, small shifts in angle for some diffraction peaks are visible in FABF/MAI/DMAI samples (Fig. 5b and Fig. S7a), indicating an expansion of crystal lattice (Fig. S7b). We also notice some differences in peak splitting. These variations confirm changes in the octahedral tilts and lattice distortions in the γ-$CsPbI_3$ structure. Further analyses of spontaneous strain formation suggests that the use of FABF/DMAI mitigates the distortions in the perovskite crystals, reducing the tilting and making it more tetragonal-like, *i.e.* β-phase (Fig. S7c).[31-32] These changes are also in line with the discrepancy of GIWAXS patterns between mXDA control and AS films (Fig. S8). As such, we conclude that the gradual formation of DMAI and FABF in the aged precursors collectively lead to a transition from orthorhombic γ-$CsPbI_3$ toward more tetragonal-like phases and hence the bandgap variations.

To generalize our findings, we investigate the ageing behaviour in other material systems. We first employ 4,7,10-trioxa-1,13-tridecanediamine (TTDDA) as the additive and prepare the devices with the respective fresh and aged solution (with a stoichiometry of PbI_2: CsI: MAI = 1: 1.15: 1).[6a, 6c] Consistent with the aromatic amines (mXDA) mentioned above, the precursors with aliphatic amines show identical positive ageing behaviour that the aged solution show red-shifted EL emission and much better performance (Fig. S9). In addition, we demonstrate that *N*-formylation of amines also occur to FA^+ involved perovskite precursors, which is confirmed by the formation of FABF in FAI/mXDA mixed DMF solution as indicated by HPLC-MS results (Fig. S10). All these results suggest that *N*-formylation widely exists in amine involved perovskite precursors. It is worthy to mention that in our previous work about TTDDA passivated $FAPbI_3$ emitters, only fresh precursor solution gives decent performance.[23] We thus

believe that the *N*-formalization of amine additives is not always positive on the device performance but a critical issue leading to varied device performance. Our findings thus call for further attention during device fabrication once amine additives are used.

In summary, we have revealed that the widely employed amine additives readily undergo *N*-formylation reaction, accompanied with hydrolysis of DMF in perovskite precursor solutions, leading to continuous changes of constitutes with storage time and thus varied device performance. Particularly, these reactions give rise to the positive ageing phenomenon in $CH_3NH_3I/CsI/PbI_2$ precursor solutions that the performance of light-emitting diodes increases with solution storage time. Our results show that the *N*-formylation and hydrolysis products collectively impact perovskite crystallization, resulting in reduced trap density and the transition from orthorhombic γ-$CsPbI_3$ toward more tetragonal-like phases. These effects hence lead to boosted electroluminescence performance and red-shifted emissions. Our results not only provide a useful strategy for fabricating deep-red $CsPbI_3$ light-emitting diodes with decent performance, but also uncover the hidden effects of chemical reactivity of amine additives on perovskite precursor solutions.

ASSOCIATED CONTENT

Supporting Information.

The Supporting Information is available free of charge on the ACS Publications website.

Experimental Details, Supplementary Scheme, Supplementary Figures and Supplementary References

AUTHOR INFORMATION

Corresponding Author

*Emial: weidong.xu@liu.se; wjzhang@szu.edu.cn; feng.gao@liu.se

Notes

The authors declare no competing financial interest.

ACKNOWLEDGMENT

We thank Dr. Xiongyu Wu (IFM, Linköping University) for his help in the reaction analysis and purification of ageing samples. We acknowledge the support from the ERC Starting Grant (No. 717026), the Swedish Government Strategic Research Area in Materials Science on Functional Materials at Linköping University (Faculty Grant SFO-Mat-LiU No. 2009-00971). This work was

financially supported by the National Natural Science Foundation of China (51472164), the 1000 Talents Program for Young Scientists of China, Shenzhen Peacock Plan (KQTD2016053112042971), and the Educational Commission of Guangdong Province (2015KGJHZ006). J.A.S. acknowledges financial support from the Research Foundation - Flanders (FWO: grant No. 12Y7221N). The authors are grateful for the collaboration of ALBA staff whom assisted with the synchrotron GIWAXS experiments performed at the NCD-SWEET beamline. F.G. is a Wallenberg Academy Fellow.

REFERENCES

(1) Liu, X. K.; Xu, W.; Bai, S.; Jin, Y.; Wang, J.; Friend, R. H.; Gao, F. Metal Halide Perovskites for Light-Emitting Diodes. *Nat. Mater.* **2021,** *20*, 10-21.

(2) Quan, L. N.; Rand, B. P.; Friend, R. H.; Mhaisalkar, S. G.; Lee, T. W.; Sargent, E. H. Perovskites for Next-Generation Optical Sources. *Chem. Rev.* **2019,** *119*, 7444-7477.

(3) Bao, C.; Xu, W.; Yang, J.; Bai, S.; Teng, P.; Yang, Y.; Wang, J.; Zhao, N.; Zhang, W.; Huang, W., et al. Bidirectional Optical Signal Transmission between Two Identical Devices Using Perovskite Diodes. *Nat. Electron.* **2020,** *3*, 156-164.

(4) Stranks, S. D.; Snaith, H. J. Metal-Halide Perovskites for Photovoltaic and Light-Emitting Devices. *Nat. Nanotechnol.* **2015,** *10*, 391-402.

(5) Tan, Z. K.; Moghaddam, R. S.; Lai, M. L.; Docampo, P.; Higler, R.; Deschler, F.; Price, M.; Sadhanala, A.; Pazos, L. M.; Credgington, D., et al. Bright Light-Emitting Diodes Based on Organometal Halide Perovskite. *Nat. Nanotechnol.* **2014,** *9*, 687-692.

(6) Xiao, M.; Huang, F.; Huang, W.; Dkhissi, Y.; Zhu, Y.; Etheridge, J.; Gray-Weale, A.; Bach, U.; Cheng, Y. B.; Spiccia, L. A Fast Deposition-Crystallization Procedure For Highly Efficient Lead Iodide Perovskite Thin-Film Solar Cells. *Angew. Chem. Int. Ed.* **2014,** *53*, 9898-9903.

(7) Liu, C.; Cheng, Y. B.; Ge, Z. Understanding of Perovskite Crystal Growth and Film Formation in Scalable Deposition Processes. *Chem. Soc. Rev.* **2020,** *49*, 1653-1687.

(8) Park, N.-G.; Zhu, K. Scalable Fabrication and Coating Methods for Perovskite Solar Cells and Solar Modules. *Nat. Rev. Mater.* **2020,** *5*, 333-350.

(9) Zhang, F.; Zhu, K. Additive Engineering for Efficient and Stable Perovskite Solar Cells. *Adv. Energy Mater.* **2019,** *10*, 1902579.

(10) Xu, W.; Lei, G.; Tao, C.; Zhang, J.; Liu, X.; Xu, X.; Lai, W.-Y.; Gao, F.; Huang, W. Precisely Controlling the Grain Sizes with an Ammonium Hypophosphite Additive for High-Performance Perovskite Solar Cells. *Adv. Funct. Mater.* **2018,** *28*, 1802320.

(11) Mahapatra, A.; Prochowicz, D.; Tavakoli, M. M.; Trivedi, S.; Kumar, P.; Yadav, P. A Review of Aspects of Additive Engineering in Perovskite Solar Cells. *J. Mater. Chem. A* **2020,** *8*, 27-54.

(12) Gao, F.; Zhao, Y.; Zhang, X.; You, J. Recent Progresses on Defect Passivation toward Efficient Perovskite Solar Cells. *Adv. Energy Mater.* **2019,** *10*, 1902650.

(13) Luo, D.; Su, R.; Zhang, W.; Gong, Q.; Zhu, R. Minimizing Non-Radiative Recombination Losses in Perovskite Solar Cells. *Nat. Rev. Mater.* **2019,** *5*, 44-60.

(14) Xue, J.; Wang, R.; Yang, Y. The Surface of Halide Perovskites from Nano to Bulk. *Nat. Rev. Mater.* **2020,** *5*, 809-827.

(15) Wu, W. -Q.; Yang, Z.; Rudd, P. N.; Shao, Y.; Dai, X.; Wei, H.; Zhao, J.; Fang, Y.; Wang, Q.; Liu, Y.; Deng, Y.; Xiao, X.; Feng, Y.; Huang, J. Bilateral Alkylamine for Suppressing Charge Recombination and Improving Stability in Blade-Coated Perovskite Solar Cells. *Sci. Adv.* **2019,** *5*, eaav8925.

(16) Chen, Z.; Zhang, C.; Jiang, X. F.; Liu, M.; Xia, R.; Shi, T.; Chen, D.; Xue, Q.; Zhao, Y. J.; Su, S., et al. High-Performance Color-Tunable Perovskite Light Emitting Devices through Structural Modulation from Bulk to Layered Film. *Adv. Mater.* **2017,** *29*, 1603157.

(17) Ono, L. K.; Liu, S. F.; Qi, Y. Reducing Detrimental Defects for High-Performance Metal Halide Perovskite Solar Cells. *Angew. Chem. Int. Ed.* **2020,** *59*, 6676-6698.

(18) Chen, B.; Rudd, P. N.; Yang, S.; Yuan, Y.; Huang, J. Imperfections and Their Passivation in Halide Perovskite Solar Cells. *Chem. Soc. Rev.* **2019,** *48*, 3842-3867.

(19) Lee, S.; Park, J. H.; Lee, B. R.; Jung, E. D.; Yu, J. C.; Di Nuzzo, D.; Friend, R. H.; Song, M. H. Amine-Based Passivating Materials for Enhanced Optical Properties and Performance of Organic-Inorganic Perovskites in Light-Emitting Diodes. *J. Phys. Chem. Lett.* **2017,** *8*, 1784-1792.

(20) Kerner, R. A.; Schloemer, T. H.; Schulz, P.; Berry, J. J.; Schwartz, J.; Sellinger, A.; Rand, B. P. Amine Additive Reactions Induced by the Soft Lewis Acidity of Pb^{2+} in Halide Perovskites. Part I: Evidence for Pb–Alkylamide Formation. *J. Mater. Chem. C* **2019,** *7*, 5251-5259.

(21) Karlsson, M.; Yi, Z.; Reichert, S.; Luo, X.; Lin, W.; Zhang, Z.; Bao, C.; Zhang, R.; Bai, S.; Zheng, G., et al. Mixed Halide Perovskites for Spectrally Stable and High-Efficiency Blue Light-Emitting Diodes. *Nat. Commun.* **2021,** *12*, 361.

(22) Cao, Y.; Wang, N.; Tian, H.; Guo, J.; Wei, Y.; Chen, H.; Miao, Y.; Zou, W.; Pan, K.; He, Y., et al. Perovskite Light-Emitting Diodes Based on Spontaneously Formed Submicrometre-Scale Structures. *Nature* **2018,** *562*, 249-253.

(23) Xu, W.; Hu, Q.; Bai, S.; Bao, C.; Miao, Y.; Yuan, Z.; Borzda, T.; Barker, A. J.; Tyukalova, E.; Hu, Z., et al. Rational Molecular Passivation for High-Performance Perovskite Light-Emitting Diodes. *Nat. Photon.* **2019,** *13*, 418-424.

(24) Tsai, H.; Nie, W.; Lin, Y.-H.; Blancon, J. C.; Tretiak, S.; Even, J.; Gupta, G.; Ajayan, P. M.; Mohite, A. D. Effect of Precursor Solution Aging on the Crystallinity and Photovoltaic Performance of Perovskite Solar Cells. *Adv. Energy Mater.* **2017,** *7*, 1602159.

(25) Yuan, Z.; Miao, Y.; Hu, Z.; Xu, W.; Kuang, C.; Pan, K.; Liu, P.; Lai, J.; Sun, B.; Wang, J., et al. Unveiling the Synergistic Effect of Precursor Stoichiometry and Interfacial Reactions for Perovskite Light-Emitting Diodes. *Nat. Commun.* **2019,** *10*, 2818.

(26) Reddy, P. G.; Kumar, G. D. K.; Baskaran, S. A Convenient Method for the N-Formylation of Secondary Amines and Anilines Using Ammonium Formate. *Tetrahedron Lett.* **2000,** *41*, 9149–9151.

(27) Ke, W.; Spanopoulos, I.; Stoumpos, C. C.; Kanatzidis, M. G. Myths and Reality of $HPbI_3$ in Halide Perovskite Solar Cells. *Nat. Commun.* **2018,** *9*, 4785.

(28) Wang, Y., Dar, M. I.; Ono, L. K.; Zhang, T.; Kan, M.; Li, Y.; Zhang, L.; Wang, X.; Yang, Y.; Gao, X.; Qi, Y.; Grätzel, M.; Zhao, Y. Thermodynamically Stabilized β-$CsPbI_3$–Based Perovskite Solar Cells with Efficiencies >18%. *Science 365*, 591–595.

(29) Steele, J. A.; Solano, E.; Jin, H.; Prakasam, V.; Braeckevelt, T.; Yuan, H.; Lin, Z.; de Kloe, R.; Wang, Q.; Rogge, S. M. J., et al. Texture Formation in Polycrystalline Thin Films of All-Inorganic Lead Halide Perovskite. *Adv. Mater.* **2021**, e2007224.

(30) Wang, Y.; Liu, X.; Zhang, T.; Wang, X.; Kan, M.; Shi, J.; Zhao, Y. The Role of Dimethylammonium Iodide in $CsPbI_3$ Perovskite Fabrication: Additive or Dopant? *Angew. Chem. Int. Ed.* **2019,** *58*, 16691-16696.

(31) Marronnier, A.; Roma, G.; Boyer-Richard, S.; Pedesseau, L.; Jancu, J. M.; Bonnassieux, Y.; Katan, C.; Stoumpos, C. C.; Kanatzidis, M. G.; Even, J. Anharmonicity and Disorder in the Black Phases of Cesium Lead Iodide Used for Stable Inorganic Perovskite Solar Cells. *ACS Nano* **2018,** *12*, 3477-3486.

(32) Yang, R. X.; Skelton, J. M.; da Silva, E. L.; Frost, J. M.; Walsh, A. Spontaneous Octahedral Tilting in the Cubic Inorganic Cesium Halide Perovskites $CsSnX_3$ and $CsPbX_3$ (X = F, Cl, Br, I). *J. Phys. Chem. Lett.* **2017,** *8*, 4720-4726.